Wind and Structures, *Vol. 28, No. 3 (2019) 155-170*
DOI: https://doi.org/10.12989/was.2019.28.3.155

Transiting test method for galloping of iced conductor using wind generated by a moving vehicle

Pan Guo[a], Dongwei Wang[b], Shengli Li[*], Lulu Liu[c] and Xidong Wang[d]

School of Civil Engineering, Zhengzhou University,
No.100 Science Avenue, Zhengzhou City, Henan Province, P.R. China. Postcode: 450001

(Received November 14, 2017, Revised December 27, 2018, Accepted January 13, 2019)

Abstract. This paper presents a novel test method for the galloping of iced conductor using wind generated by a moving vehicle which can produce relative wind field. The theoretical formula of transiting test is developed based on theoretical derivation and field test. The test devices of transiting test method for aerodynamic coefficient and galloping of an iced conductor are designed and assembled, respectively. The test method is then used to measure the aerodynamic coefficient and galloping of iced conductor which has been performed in the relevant literatures. Experimental results reveal that the theoretical formula of transiting test method for aerodynamic coefficient of iced conductor is accurate. Moreover, the driving wind speed measured by Pitot tube pressure sensors, as well as the lift and drag forces measured by dynamometer in the transiting test are stable and accurate. Vehicle vibration slightly influences the aerodynamic coefficients of the transiting test during driving in ideal conditions. Results of transiting test show that the tendencies of the aerodynamic coefficient curve are generally consistent with those of the wind tunnel tests in related studies. Meanwhile, the galloping is fairly consistent with that obtained through the wind tunnel test in the related literature. These studies validate the feasibility and effectiveness of the transiting test method. The present study on the transiting test method provides a novel testing method for research on the wind-resistance of iced conductor.

Keywords: transiting test method; moving vehicle; iced conductor; aerodynamic characteristic; wake galloping; wind tunnel test

1. Introduction

Galloping is a wind-induced oscillation of high-voltage transmission lines characterized by large amplitude and low frequency, which are detrimental to the safety of electrical lines. The ice accretion on the conductor changes the cross-section of the conductor in most cases. Thus, the conductor becomes aerodynamically unstable and galloping then occurs. Wind tunnel test, numerical simulation and field test are currently the most commonly used methods to study the wind-induced vibration characteristics of iced conductor. The wind tunnel test is an important means of obtaining the aerodynamic coefficients of iced conductor and has been used to estimate the property of iced conductor under the action of natural wind (Guo *et al.* 2019, Zhou *et al.* 2016, Ma *et al.* 2015, Yan *et al*. 2014). However, wind tunnel test is costly, and the airflow boundary in the wind tunnel objectively exists, which leads to a difference from the natural wind field due to the influence of the streamline curvature near the boundary (Yousef *et al*. 2018, Khayrullina *et al*. 2015, Choi *et al.* 1998). Numerical simulation is more rapid and more economical than the wind tunnel test. Owing to the rapid development of computer technology, numerous scholars have adopted numerical methods to study the galloping of noncircular section conductor (Guo *et al.* 2017, Li *et al.* 2017, Xu *et al.* 2015, Chen *et al*. 2015, Cai *et al.* 2015, Alonso *et al.* 2007, Shuji Shirai *et al.* 2003).

However, the precision of the computational results is most significantly affected by factors such as boundary condition, physical parameter, and post-processing method. The results of existing research show that the CFD simulation results can qualitatively react to the change trend of the aerodynamic performance of iced conductor to some degree, and the numerical values are different from those of the wind tunnel test. Field measurement is influenced by the objective environment and thus is generally not preferred as a method for structure wind-resistant (Wen *et al*. 2018, Feng 2018, Wang *et al*. 2013). In summary, wind tunnel tests, numerical simulations, and field measurements of iced conductor wind resistance have their respective advantages and disadvantages as research methods. The wind tunnel test requires a large wind-tunnel laboratory and high costs, thereby severely limiting the scientific research of structural wind resistance analysis. Therefore, the development of a portable wind-resistance test method has considerable significance.

According to the relativity of movement, a relative wind field can be easily generated around a vehicle during

[*]Corresponding author, Associate Professor,
E-mail: lsl2009@126.com
[a] Ph.D.,
E-mail: 77741289@qq.com
[b] Professor,
E-mail: dongweiwang@zzu.edu.cn
[c] Master Student,
E-mail: 643626951@qq.com
[d] Ph.D.,
E-mail: xidong.wang@zzu.edu.cn

http://www.techno-press.com/journals/was&subpage=7 ISSN: 1226-6116 (Print), 1598-6225 (Online)

driving. The airflow field around the vehicle will be substantially influenced during driving, and the objects fixed on the vehicle surface will then be affected by the wind. The wind is generated by the moving vehicle, and the wind speed and direction are closely related to the speed and route of the vehicle. Knight *et al*. (2010) studied deformation and pressure distribution of car roof under different wind speeds through numerical simulation and proposed a numerical simulation method based on linear element model. Wang *et al.* (2010) analyzed the effects on the grip of the car by the front and rear wings under different ground clearances and wind speeds through numerical simulation and wind tunnel test. Tao *et al*. (2015) studied the wind-induced vibration characteristics of a car windshield under different wind speeds by numerical simulation and wind tunnel. Blocken *et al.* (2015) studied the running resistance of bicycles with a car following, and the results of their numerical simulation and wind tunnel test showed that a moving car not only affects its surrounding flow field but also other surrounding objects. Yang *et al.* (2015) analyzed the pressure distribution of a bridge when a high-speed train passes under it by means of field measurement and numerical simulation. The preceding studies mentioned showed that the entire or part of the vehicle body and the transported objects are affected by wind generated by a moving vehicle.

Recently, some scholars have adopted transiting test method to carry out relevant research, and and achieved good results. For example, Altinisik (2017) studied the drag coefficients of passenger car by transiting tests, and the results are in good agreement with the CFD results and wind tunnel results. Skrúcaný *et al*. (2018) found that the rolling coefficient values of truck by transiting test are very similar to the declared value by tire producer.

Inspired by the relevant research results, this paper proposes a type of transiting test method that uses wind generated by a moving vehicle to test the galloping of iced conductor in ideal conditions. The theoretical formula of the transiting test method is developed on based on theoretical derivation and field test. The test devices of the transiting test method for aerodynamic coefficient measurement and galloping of iced conductor are designed and assembled, respectively. The aerodynamic characteristics and galloping of iced conductor are then studied using the transiting test method. The present study on the transiting test method provides a novel testing method for wind resistance research of iced conductor.

2. Transiting test method

2.1 Basic hardware and software system

As shown in Fig.1, the basic hardware system of the transiting test method includes a car with cruise control function, a test platform fixed on the car roof, a rigid steel support, a test model, a Pitot tube, vibration pickup sensors, a notebook computer, power supply equipment, and a regulating device of wind attack angle.

The test platform fixed on the car roof is a steel plate with a size of 90 mm × 60 mm × 5 mm. The required bolt holes are set to fix the rigid steel support (Fig. 1(a)). The power supply equipment comprises lead-acid batteries, a charger, and an inverter. The car with cruise control function is the 2011 FAW-VW Bora. The specimen of iced conductor and the rigid steel support are modified to accommodate the requirements of the experiment.

The Pitot tube used to test the total and static pressures of the relative wind field in the test (Fig. 1) is on the right front of the test platform. A standard L-shaped Pitot tube produced by the Shanghai Reynolds Instrument Technology Co., Ltd., China is selected in the test, and the tube is 6 mm in diameter and 50 cm long. The diameter of the hole used to test the static and total pressures is 2.5 mm. The high-frequency pressure sensors (Xi'an Beauty Technology Co., Ltd., China) corresponding to the Pitot tube are used to measure the total and static pressures. The range is ±2 KPa, the accuracy is 0.25%, and the highest frequency is approximately 4 KHz. The pressure sensors are connected to the computer via a USB.

In the transiting test, the vibration pickup sensors (see Fig. 1(a)) are used to obtain the vibration acceleration of the test model to determine the influence of car vibration during driving on the test results. The vibration pickup sensors provided by the China Orient Institute of Noise & Vibration are used in the vibration test. In the transiting test, two acceleration vibration testers are used to test the vibration accelerations in the direction of lift and drag, and a sampling frequency of 128 Hz is adopted.

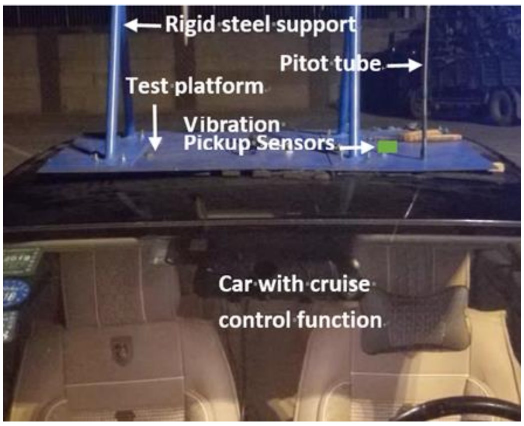

(a) Basic hardware system of the transiting test method

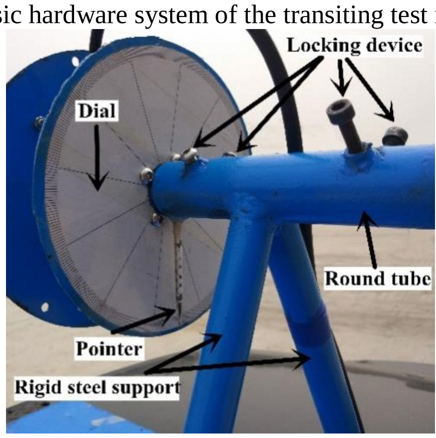

(b) Regulating device of wind attack angle

Fig. 1 Basic test device of the transiting test method

Table 1 Ideal test conditions

Project	Limitations	Assumptions
Road conditions	Smoothness, IRI (m/km) ≤2.0, length of straight line ≥2 km	Ignore the effects of road cross-sectional slope, pavement roughness, road greening, and surrounding buildings
Weather conditions	Temperature 25±10°, Humidity <58%	
Surrounding environment	No other vehicles	
Natural wind	<1 m/s	
Vehicle conditions	The vehicular speed is uniform. The vehicles move in a straight line and in the middle lane.	Ignore the effects of engine wobble
Test platform conditions	Positioned horizontally	Ignore the interference of the screw heads on the platform
Wind profile	Ignore	
Turbulence intensity	≤1%	

The regulating device of the wind attack angle (Fig. 2(a)) is a circular turntable with a scale. A dial is painted on the lower surface of the circular turntable, and a pointer is arranged at the end of the round tube above the bracket to accurately adjust the wind attack angle. The locking device comprises four screws passing through the outer wall of the round tube and the center of the circle. The regulating accuracy of wind attack angle is 1°.

The basic software system of the transiting test method presented in this paper includes a Windows 7 operating system for computer, data collection and processing software, and management software. The basic data collection and processing software are intended for high-frequency pressure sensors and the vibration pickup sensors. Other software will be designed and installed to cater to the experimental requirements.

2.2 Ideal condition and selection of test road

The transiting test is still at a preliminary stage. Hence, numerous external influences are inevitable, and factors such as road type, surrounding environment, external natural wind, and vehicle condition will affect the test results. Therefore, the test is limited to the ideal test conditions.

The ideal test conditions shown in Table 1 are as follows: minimal or no vehicle vibration, flat and straight road, minimal or ignorable natural wind, no surrounding traffic, and sufficient distance between the test model and the test platform on the car roof.

A fast-paced highway could be selected in this study to meet the ideal test conditions. The transiting test could be performed on a straight and flat section of the road, while the natural wind could be ignored. The test model is sufficiently far from the test platform on the car roof, and the car cruise control function is used to ensure steady speed.

The straight sections in Zheng Yun high-speed route (Wuzhi to Yuntai Mountain, Henan, China) with nearly no traffic flow, as well as the presence of natural wind, are selected in accordance with the preceding requirements provided. Zheng Yun Expressway, which is a new expressway opened to traffic on November 26, 2016, is 36 km long and has a design speed of 100 km/h, as shown in Figs. 2 and 3). The road is flat and straight and is located in the Central Plains region, which is surrounded by open space. The highway segments whose design indexes to meet the ideal test conditions and which are adopted in transiting tests are shown in Table 2.

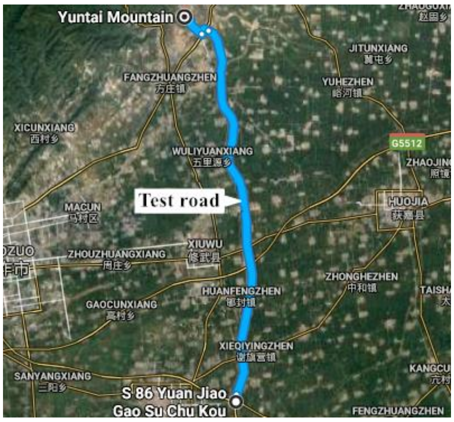

Fig. 2 Wuzhi to Yuntai Mountain section of Zheng-Yun high-speed route, Henan, China

Fig. 3 Photo of Zheng-Yun high-speed route

Table 2 Design indexes of the Wuzhi to Yuntai Mountain section in Zheng-Yun high-speed route

Mileage stake number	Horizontal curve elements	Vertical curve elements
K8+185~K12+575	straight line	<1.5%
K19+446~K22+075	straight line	<1.0%
K25+900~K28+000	straight line	<1.0%
K31+600~K33+650	straight line	0.88%

2.3 Test procedure

The flowchart of the transiting test method is shown in Fig. 4. First, a suitable test road and test periods are selected. The car is started after installing and debugging the test platform and the equipment. The car is driven and stabilized at test speed, and the cruise control is switched on to facilitate car travel at test speed. Then, the test data of each test condition are collected and preliminarily assessed. Finally, after recording all test data, the test is completed, the car is stopped, and the test platform and test equipment are dismantled.

3. Transiting test method for aerodynamic coefficient measurement of iced conductor

3.1 Theory of aerodynamic coefficient measurements for transiting test method

The aerodynamic coefficients of the test model can be expressed according to the wind tunnel tests as follows (Nigol 1981)

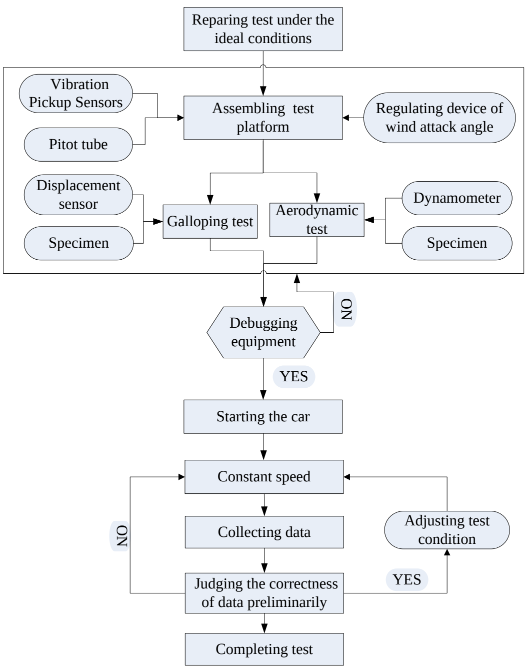

Fig. 4 Flowchart of the transiting test method

$$C_D = \frac{2F_D}{\rho U^2 Ld} \tag{1}$$

$$C_L = \frac{2F_L}{\rho U^2 Ld} \tag{2}$$

$$C_M = \frac{2M}{\rho U^2 Ld^2} \tag{3}$$

where , C_D, C_L, and C_M respectively denote the drag force coefficient, the lift force coefficient, and the moment coefficient. F_D, F_L, and M represent the drag force, the lift force, and the moment, respectively. ρ is the air density, and U is the wind speed. L is the effective length of iced conductor, and d is the diameter of the conductor.

A Pitot tube and pressure sensors are used to directly test the wind speed and measure the total and static pressures. The wind speed can be calculated based on the Bernoulli equation presented as follows

$$U = \sqrt{\frac{2(P_0 - P)}{\rho}} \tag{4}$$

where, U is the speed of the wind generated by a moving vehicle, P_0 is the total pressure, P is the static pressure, and ρ is the air density.

The following formulas can be obtained after a series of calculations by means of putting formula (4) into formula (1), (2) and (3).

$$C_D = \frac{F_D}{(P_0 - P)Ld} \tag{5}$$

$$C_L = \frac{F_L}{(P_0 - P)Ld} \tag{6}$$

$$C_M = \frac{M}{(P_0 - P)Ld^2} \tag{7}$$

Eqs. (5)- (7) are the basic theoretical formulas of the transiting test method for the aerodynamic coefficient measurements of iced conductor. Owing to the differences in the traditional expressions of the aerodynamic coefficients in the wind tunnel tests and numerical simulations, the air density need not be measured in the transiting test. Accordingly, temperature, altitude, and other influencing factors of air density cannot indirectly affect the transiting test results. The theoretical formulas of the transiting test method in this study are simple and practical.

3.2 Special Hardware and software system for the aerodynamic coefficient measurements

The hardware system (Fig. 5) of the transiting test method for the aerodynamic coefficient measurements of iced conductor includes a dynamometer and the specimen of the iced conductor.

The dynamometer (Model NOS-C901 produced by Changsha Nor Sai Heath Instrument Co., Ltd., China) is used to measure the aerodynamic force model test. The X- and Y-axis force range is ±150 N, and the Z-axis moment range is ±50 N·m. The sampling frequency used is around 10 Hz. The single-path accuracy is 0.5%, and the overall accuracy is below 2.5%. The dynamometer can be connected to a computer via a USB to enable convenient storage and data processing. A software system named “three-dimensional force software processing system” corresponding to the dynamometer is shown in Fig. 6.

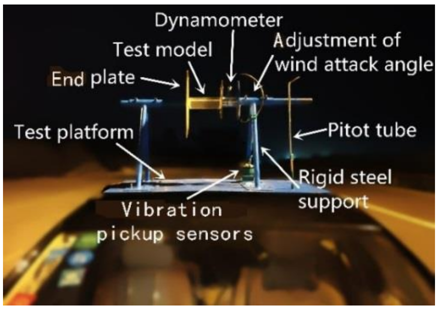

Fig. 5 Test device of the transiting test method for aerodynamic coefficients of iced conductor

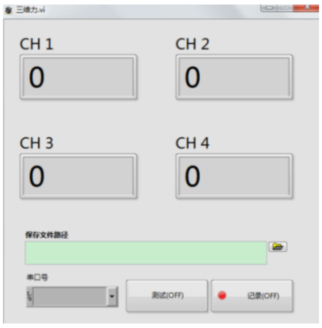

Fig. 6 Three dimensional force software processing system corresponding to the dynamometer

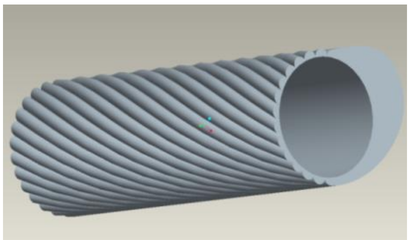

(a) 3D mode of the iced conductor

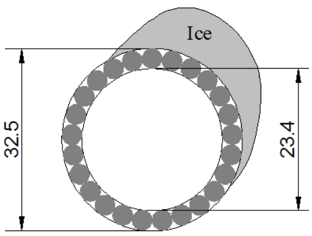

(b) Shape of the specimen section (unit: mm)

Fig.7 Specimen of the iced conductor for aerodynamic coefficient measurements

The size of the iced conductor specimen for aerodynamic coefficient measurements is identical with that of the benchmark model adopted in Reference (Chabart *et al*. 1998), and the specimen is made of lightly cured composite resins with 3D printing. The length of the specimen is 0.2 m (Fig. 7(a)), and its eccentricity, that is, the ratio between ice thickness and radius of the conductor, is 1.32. The distance between the center of gravity of the ice and the center of the cable is 2.17×10^{-2} m (Fig. 7(b)).

3.3 Results and analysis

3.3.1 Test and analysis of the wind speed generated by a moving vehicle

The wind generated by a moving vehicle has stochastic and time-varying characteristics, which are considered incompressible. Based on the Pitot tube principle used to measure fluid velocity in hydromechanics and Eq. (4), the wind speed can be measured by calculating the difference between the total hydro and static pressures when the air density is constant. Therefore, fluctuation of wind speed during the experiments can be reflected by the time-course curve of the difference between the total hydro and static pressures as well as the spectrograph.

Due to space limitations and topics, three sets, which are randomly sampled from vast quantities of data when the vehicle speed is 47 km/h (13 m/s) for 3 minutes in the ideal conditions and the data is acquired simultaneously (three times), are analyzed and shown in Fig. 8. The difference between the total hydro and the static pressures generated by a moving vehicle at 47 km/h (13 m/s) is relatively stable according to the time-history curve of the difference and the frequency spectrum graphics. Moreover, the driving wind field is stable in the transiting test and has relatively less interference from the external factors under ideal conditions. This result indicates that the driving wind field can be considered in the experimental investigation of wind-resistant structures.

3.3.2 Analysis of vehicular vibration

Automobile is a complex vibration system including vertical, longitudinal angle, roll, and engine vibrations (Burdzik *et al*. 2017). The vibration inertia force which is simultaneously collected by the dynamometer at the same time will be superimposed on the aerodynamic force in the transiting test. In this paper, the influence of the vehicle vibration on the transiting test is studied through experimental research.

The values measured by the dynamometer include aerodynamic and vibration inertial forces when the wind generated by a moving vehicle is used to measure aerodynamic forces. The vibration time history of the test model can be collected by the vibration pickup sensors during driving. Owing to the direction of the drag force is consistent with the vehicle direction and mainly affected by whether the vehicle runs straight or not, so the influence of the vibration inertial force in the vehicle direction can be negligible. The influence of the vibration inertial force on the lift results are analyzed and discussed in this subsection.

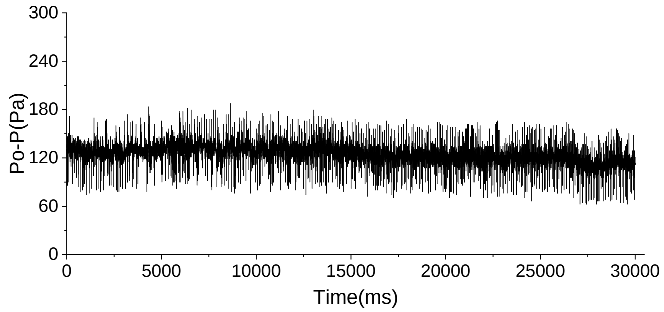

(a) Time-course curve of the difference between the total hydroand static pressures

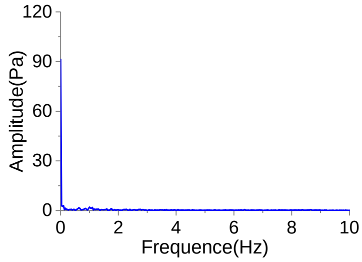

(b) Spectrograph of the difference between the total hydro and static pressures

(1) First test

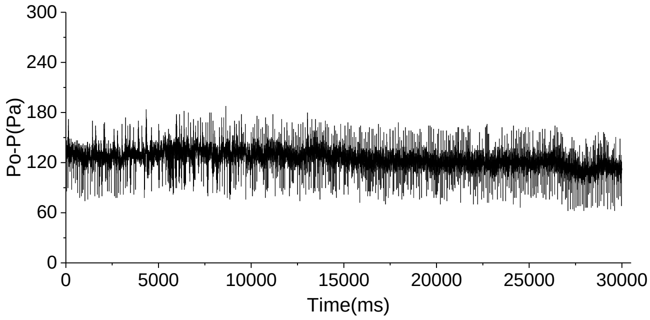

(a) Time-course curve of the difference between the total hydroand static pressures

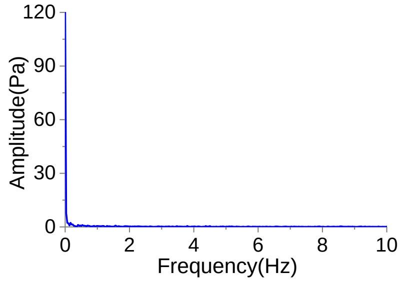

(b) Spectrograph of the difference between the total hydro and static pressures

(2) Second test

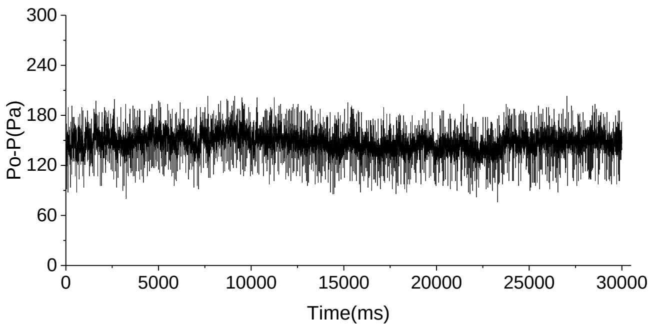

(a) Time-course curve of the difference between the total hydroand static pressures

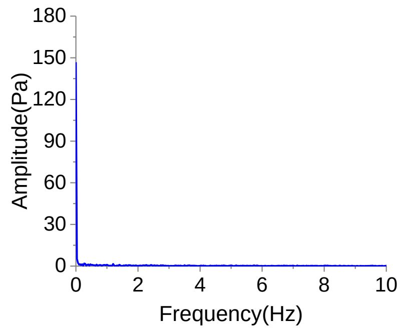

(b) Spectrograph of the difference between the total hydro and static pressures

(3) Third test

Fig. 8 Analysis diagram of the difference between the total hydro and static pressures generated by a moving vehicle at 47 km/h under ideal conditions based on three tests and 30 s collection time interval

The historical diagram and spectrogram of the lift force and the vibration accelerations in the direction of lift are shown in Fig. 9. The test speed is 47 km/h (13 m/s) under ideal conditions. The collection time is 180 s, and the wind attack angles are 150°, 162°, and 180° (Fig. 9). As shown in Fig. 9, the results of dynamometer measurements are stable with minimal fluctuation. Under different conditions, the predominant frequency of the vibration accelerations in the lift direction ranged from 9.5 Hz to 10 Hz, while that of the lift force is not more than 0.5 Hz. All these results suggest that the inertial force generated by the vehicular vibration is extremely small and negligible relative to aerodynamic force under ideal conditions.

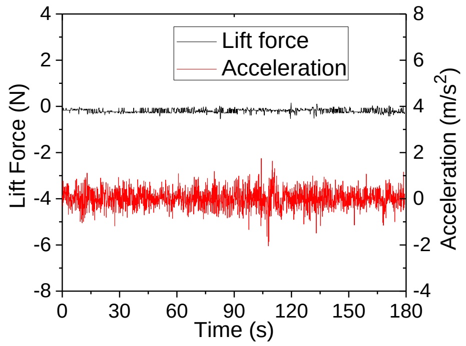

(a) Historical diagram

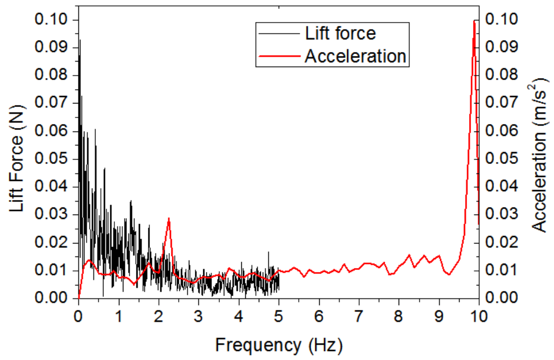

(b) Spectrogram

(1) Historical diagram and spectrogram with 150° wind attack angle

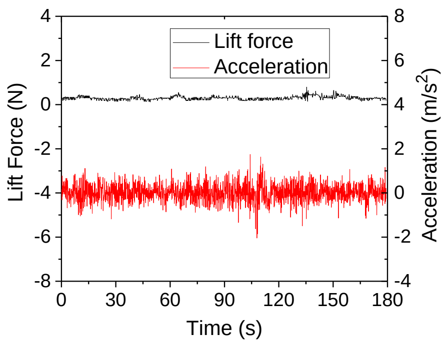

(a) Historical diagram

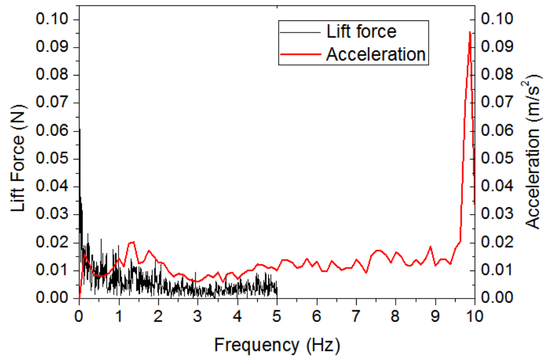

(b) Spectrogram

(2) Historical diagram and spectrogram with 162° wind attack angle

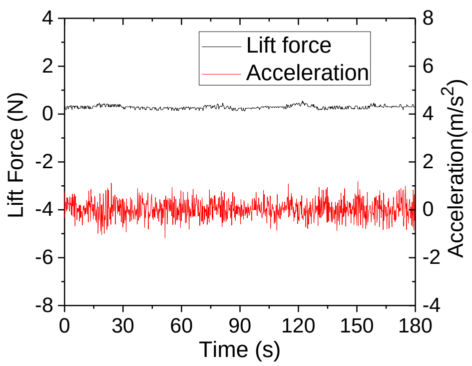

(a) Historical diagram

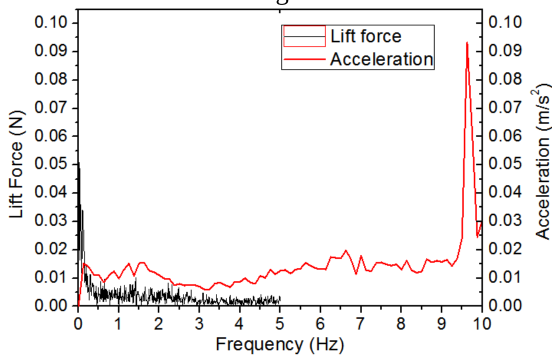

(b) Spectrogram

(3) Historical diagram and spectrogram with 180° wind attack angle

Fig. 9 The history diagram and spectrogram of the lift force and the vibration accelerations in the direction of lift with different wind attack angles (47 km/h speed)

3.3.3 Analysis of aerodynamic coefficients

In order to verify the correctness and the feasibility of the transiting test method for aerodynamic coefficient measurements of iced conductor and prepare for the study of galloping, the aerodynamic coefficients are analyzed and discussed in this subsection.

The size of iced conductor specimen for aerodynamic coefficient measurements is identical with that of the benchmark model size adopted in reference (Chabart *et al*. 1998). However, a few of the benchmark model sizes adopted in reference (Chabart *et al*. 1998) were not clearly defined, such as the form of icing on the conductor and the size of the thin wire, and materials used in the test were different from those in reference (Chabart *et al*. 1998). Therefore, the correlation analysis results were not only compared with the results of reference (Chabart *et al*. 1998) but also with other similar results to test the accuracy of the testing methods in this study (Nigol 1974, Wang *et al*. 2011). Owing to the differences between the size and material of specimens, features and change rules of the same kind of iced conductor are investigated by qualitative analysis. The cross-section shape of iced conductor in previous studies is shown in Fig. 10, and the aerodynamic coefficient curves of lift and drag are shown in Figs. 11(a) and 11(b), respectively.

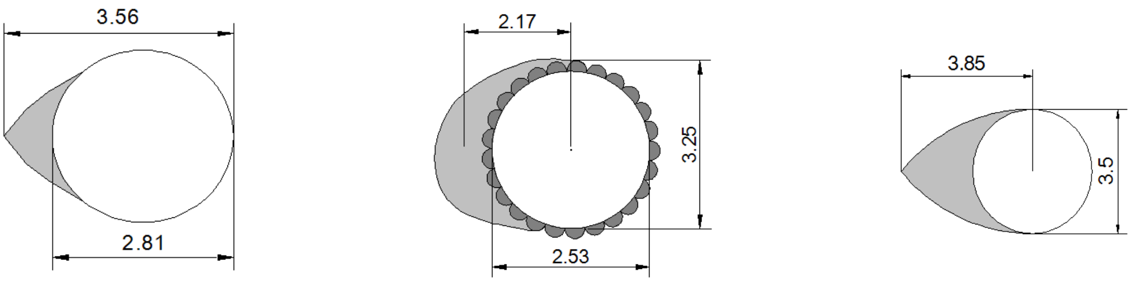

(a) Nigol (1974) (b) Chabart (2000) (c) Wang (2011)

Fig. 10 The cross section shape of iced conductor in previous studies (unit: cm)

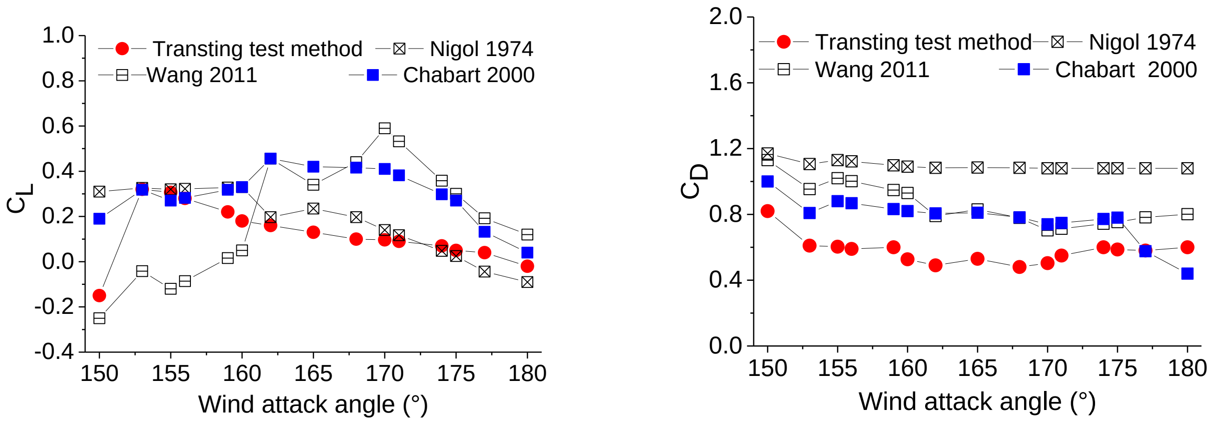

(a) Lift coefficient curves (b) Drag coefficient curves

Fig. 11 Aerodynamic coefficient curves of different tests

As shown in Figs. 11(a) and 11(b), based on the comparison of the aerodynamic coefficient curves of lift and drag in this study and those of other studies, the changing trends of the curves are basically the same, which confirms the feasibility of the proposed methods. The lift coefficient in the range of 150°–180° rises from top to bottom and forms a wave crest, but the drag coefficients are relatively stable. The result of (c) study is quite different from the test because the ice is thin and the shape is smooth. The lift coefficient curve of test (c) is not evident in the range of 150°–180°, no wave crest is formed, and the drag coefficient decreases.

The preceding discussion and analysis reveal that the size of the iced conductor specimen for aerodynamic coefficient measurements is identical with that of the benchmark model size adopted in reference (Chabart *et al.* 1998), namely (b) study. However, the amounts of data provided in the present study are generally less. This observation can be attributed to the following reasons. 1) A dynamometer was used to measure the spring and derive the aerodynamic coefficients of ice conductor in (b) study, whereas the iced conductor model in the present study was directly measured by a dynamometer. 2) The difference of specimen material leads to different levels of roughness of specimen surface (An et al. 2016). 3) A few sizes in (b) study were not clearly defined, such as the form of icing on the conductor and the size of the thin wire.

4. Transiting test method for galloping measurements of iced conductor

4.1 Galloping theory

According to the galloping mechanism of Den Hartog (Fig. 12), vibration in the Y direction will occur under the action of wind speed U, and the velocity of vibration is $\dot{y}$. The motion equation can be expressed as in Eq. (8) when the wind attack angle is α.

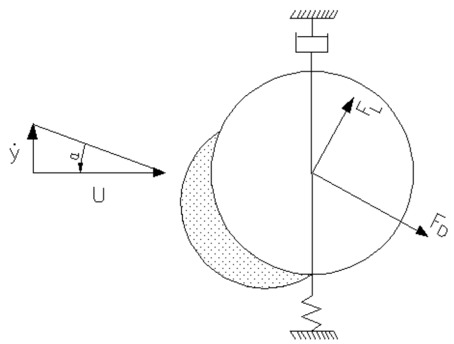

Fig. 12 Den Hartog's galloping model of iced conductor

$$\ddot{y}+[2\varepsilon_y\omega_y+\frac{U\rho d^2}{2d}(\frac{\partial C_L}{\partial \alpha}+C_D)]\dot{y}+\omega_y^2 y=0 \quad (8)$$

where, ω_y is the vertical natural frequency, ε_y is the vertical natural damping ratio, and ρ is the air density.
The DenHartog criterion is important to determine the occurrence of galloping in a structure. The concept of galloping coefficients is expressed as follows (Den 1932)

$$A=\frac{\partial C_L}{\partial \alpha}+C_D<0 \quad (9)$$

where, the Den Hartog coefficient A is equal to the sum of the drag coefficient and the derivative of the lift coefficient on the wind attack angle.

4.2 Special Hardware and software system for galloping measurements

As shown in Fig. 13, the device of the transiting test method for galloping measurements of iced conductor includes springs and laser displacement sensor. The test specimen made of lightly cured composite resins with 3D printing is suspended by four vertical springs, which are prestressed to limit the static deformation due to the deadweight of the structure (2.99 kg) (Fig. 13). Meanwhile, four horizontal springs allow the horizontal oscillation of the system. The stiffness of all the springs is 14 N/m. The length of the artificial ice is 0.8 m (Fig. 14), and the section size is shown in Fig. 7. The horizontal and vertical damping of the device tested by logarithmic decay are less than 0.08%. A total of two closed boxes are directly placed at the extremities of the ice sample (Fig. 15) to prevent the wind from blowing on the springs and the part of the structure without ice, and two rectangles with a size of 200 mm × 300 mm openings on the inside surface allow sample movement while limiting the maximum amplitude.

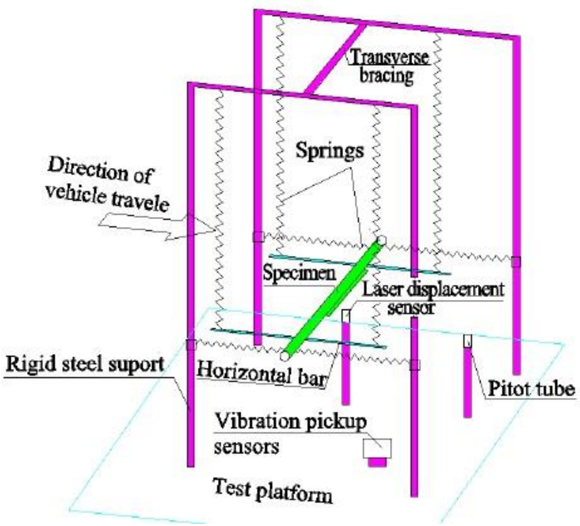

Fig. 13 Diagram of galloping measurement device of iced conductor in transiting test

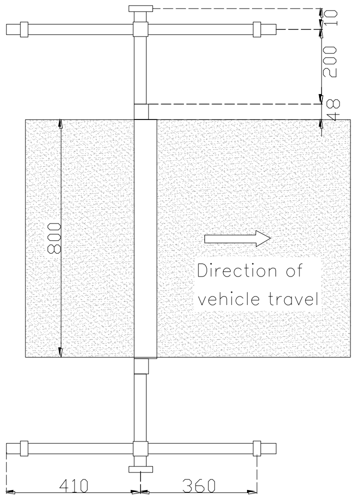

Fig. 14 Technical representation of the suspended test sample(unit: mm)

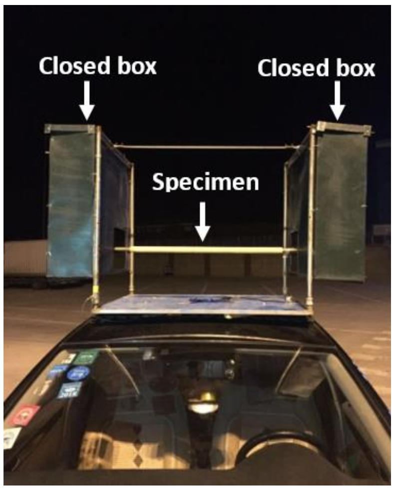

Fig. 15 Galloping measurement device of iced conductor in transiting test

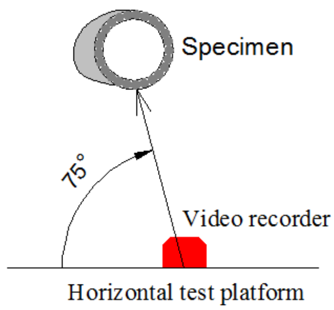

Fig. 16 Shooting angle in transiting test

The vertical displacements of the sample are recorded via a diffusion reflective laser displacement sensor working at 100 Hz sampling frequency, 300 μm resolution, and 300±200 mm detection distance.

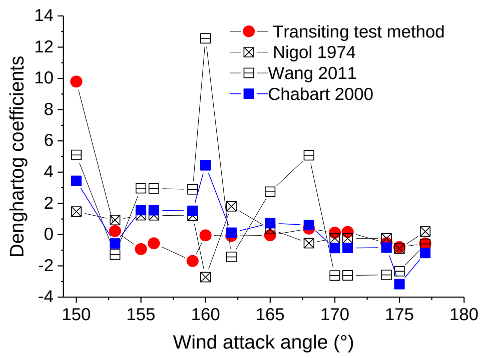

Fig. 17 DenHartog coefficients of iced conductor

The vibrating trace of the sample is recorded by means of a video recorder working with a resolution of 829 pixels which is placed on the test platform, and the shooting angle is 75°from Horizontal level (Fig. 16).

4.3 Test condition of transiting test method for galloping measurements of iced conductor

Based on the analysis of the 4.1 section, Below-zero Den Hartog coefficients are requirements for the occurrence of galloping in iced conductor. The Den Hartog coefficient can be calculated using the aerodynamic coefficients of lift and drag presented in Section 3.4.3, as shown in Fig. 17.

The galloping coefficients shown in Fig. 17 are consistent and less than zero for a wind attack angle range of 174° to 180°. The iced conductor may cause the occurrence of galloping during construction in the wind attack angle range of 174° to 180°.

The transiting test for galloping measurements of iced conductor is done in Zheng Yun high-speed route (Wuzhi to Yuntai Mountain, Henan, China) (see Table 2) according to the test process (see Fig.4) in the ideal conditions (see Table 1), and the test condition of wind attack angle of 180° is selected for the present study.

4.4 Results and analysis

As shown in Fig. 18, the size of the specimen is increased, the amplitude of vertical vibration is see-sawed, and the maximum amplitude is 7.5 mm when the speed is 40 km/h and the wind attack angle of the specimen is 180° under ideal conditions.

As shown in Fig. 19, when the speed is 45 km/h and the wind attack angle of the specimen is 180°under ideal conditions, the vertical vibration amplitude of the iced conductor gradually increases over time. The maximum amplitude that appeared at around 180 s is 45 mm, which is considerably short of the limit value in the test. The amplitude gradually decreases after reaching the maximum value.

When the speed is 46 km/h and the wind attack angle of the specimen is 180° under ideal conditions, the vertical vibration amplitude of the iced conductor gradually increases over time. The maximum amplitude that appeared at around 136 s is 57 mm, which is significantly short of the limit value in the test. The amplitude gradually decreases after reaching the maximum value, and the maximum amplitude appears again after a time interval of 50 s (see Figs. 20 and 21).

When the speed is 47 km/h and the wind attack angle of the specimen is 180° under the ideal conditions, the iced conductor continues to shake at 10 cm from the end of the limit hole and exhibits a tendency for divergence. The galloping occurs and the iced conductor establishes contact with the upper limit of the hole at around 138 s. Then, the amplitude gradually decreases (see Figs. 22 and 23).

When the speed is 50 km/h and the wind attack angle of the specimen is 180° under ideal conditions, the iced conductor continues to shake at 12 cm from the end of the limit hole and exhibits a tendency for divergence. The galloping occurs and the iced conductor rapidly diverges and establishes contact with the upper limit of the hole after a slight shock of approximately 25 s. Then, the amplitude gradually decreases (see Figs. 24 and 25).

When the speed is 55 km/h and the wind attack angle of the specimen is 180° under ideal conditions, the amplitude starts to rapidly diverge when the iced conductor stabilizes at 15 cm from the end of the limit hole. The galloping occurs and the iced conductor rapidly diverges and establishes contact with the upper limit of the hole after a slight shock of approximately 10s. Then, the amplitude gradually decreases (see Figs. 26 and 27).

The preceding analysis demonstrates that when the speed is less than 47 km/h and the wind attack angle of the specimen is 180° under ideal conditions, the time to maximum amplitude tends to occur early as the speed increases, while the amplitude gradually increases but exhibits no divergent tendency, and the specimen does not suffer from galloping. By contrast, when the speed is greater than or equal to 47 km/h, the amplitude with divergent tendency gradually increases, and the galloping of the specimen occurs. The result also indicates that as the speed increases, the consumption time for galloping occurrence gradually decreases, and the distance gradually moves farther away from the end of the limit hole.

5. Discussion

5.1 Relationship between the driving speed and the wind speed generated by the moving vehicle

The dashboard data for vehicular speed is obtained by wheel speed through Electronic Stability Program (ESP). However, owing to the precision problem of ESP sensors, a difference exists between the driving speed and the wind speed generated by the moving vehicle, while a test error exists for the rotation speed and the external wind speed.

Article 4 of "Speed meters for motor vehicle", which is the national standard of China (GB 15082-2008), states that the relationship between the indicated speed (v_1) and the actual speed (v_2) shall meet Eq. (10).

$$0 \le v_1 - v_2 \le \frac{v_2}{10} + 4 \tag{10}$$

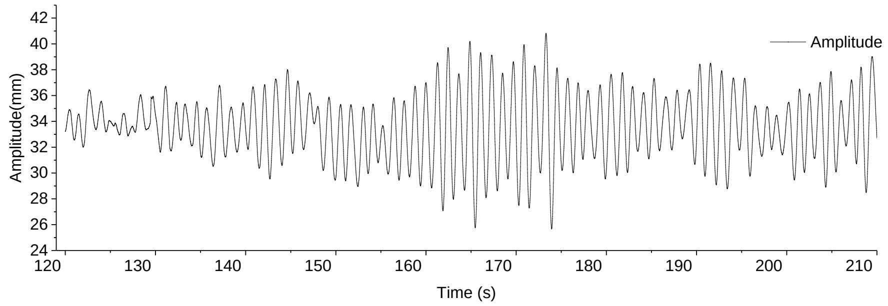

Fig. 18 Vertical displacement - time diagram of the specimen when the speed is 40 km/h and the wind attack angle of the specimen is 180° under ideal conditions

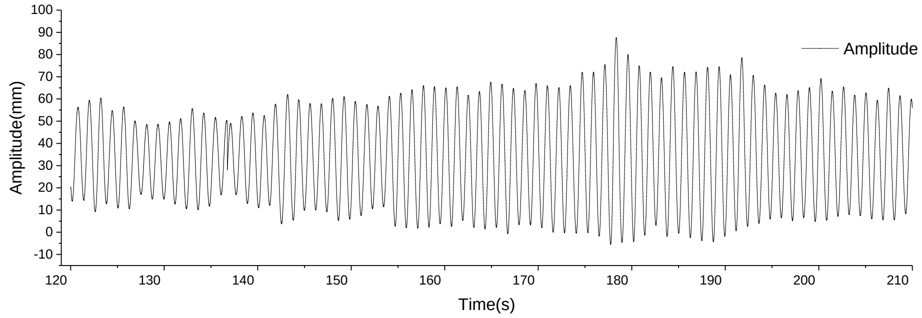

Fig. 19 Vertical displacement - time diagram of the specimen when the speed is 45 km/h and the wind attack angle of the specimen is 180° under ideal conditions

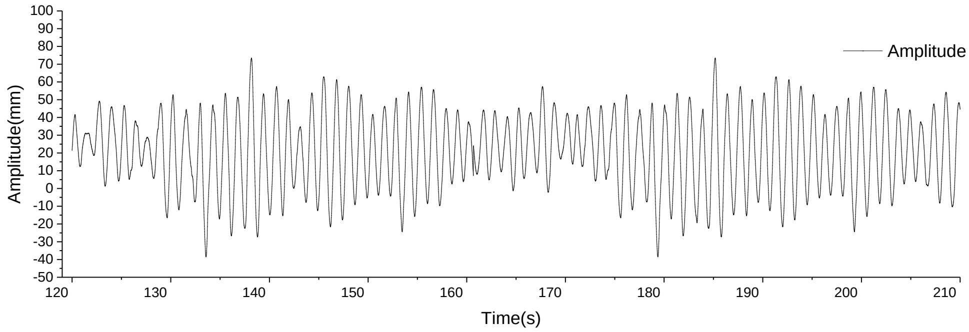

Fig. 20 Vertical displacement - time diagram of the specimen when the speed is 46 km/h and the wind attack angle of the specimen is 180° under ideal conditions

(a) Minimum displacement screenshot(unit: mm) (b) Maximum displacement screenshot(unit: mm)

Fig. 21 Extreme displacement screenshots of the specimen when the speed is 46 km/h and the wind attack angle of the specimen is 180° under ideal conditions

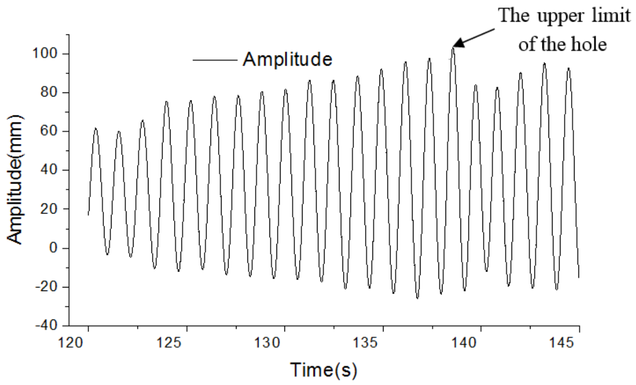

Fig. 22 Vertical displacement - time diagram of the specimen when the speed is 47 km/h and the wind attack angle of the specimen is 180° under ideal conditions

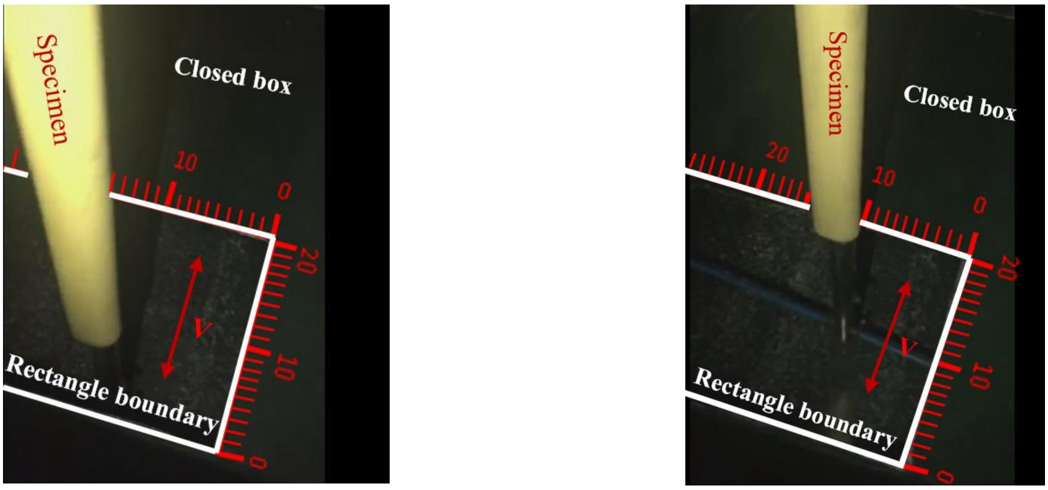

(a) Minimum displacement screenshot(unit: mm) (b) Maximum displacement screenshot(unit: mm)

Fig. 23 Extreme displacement screenshots of the specimen when the speed is 47 km/h and the wind attack angle of the specimen is 180° under ideal conditions

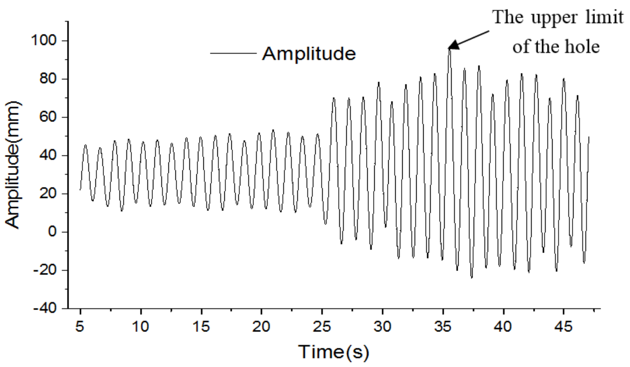

Fig. 24 Vertical displacement - time of the specimen when the speed is 50 km/h and the wind attack angle of the specimen is 180° under ideal conditions

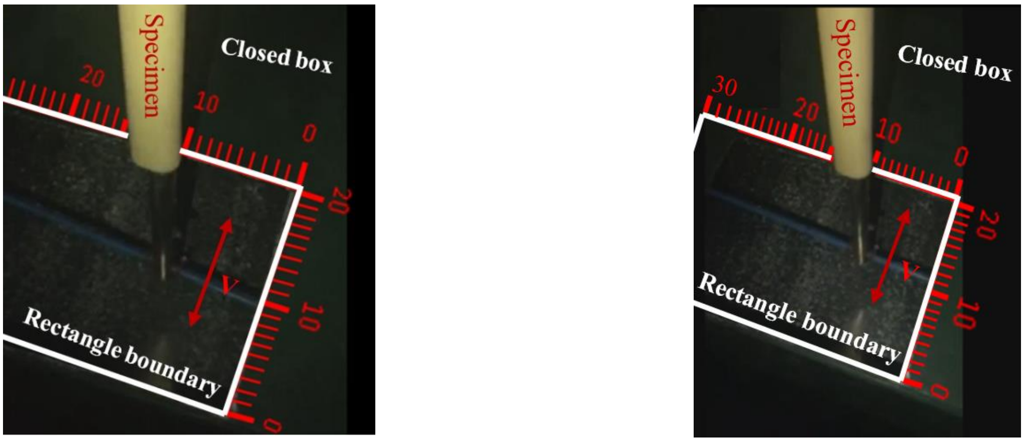

(a) Minimum displacement screenshot(unit: mm) (b) Maximum displacement screenshot(unit: mm)

Fig. 25 Extreme displacement screenshots of the specimen when the speed is 50 km/h and the wind attack angle of the specimen is 180° under ideal conditions

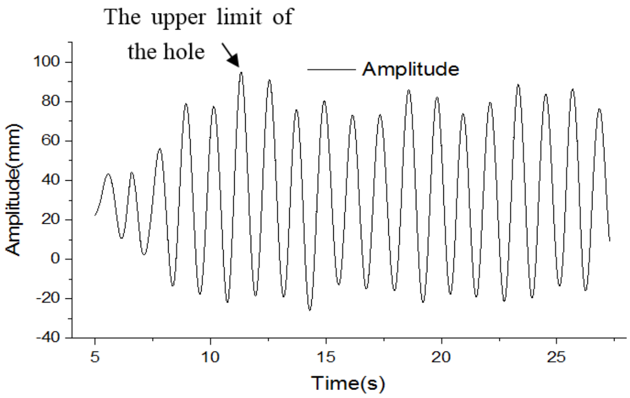

Fig. 26 Vertical displacement - time diagram of the specimen when the speed is 55 km/h and the wind attack angle of the specimen is 180° under ideal conditions

(a) Minimum displacement screenshot(unit: mm) (b) Maximum displacement screenshot(unit: mm)

Fig. 27 Extreme displacement screenshots of the specimen when the speed is 55 km/h and the wind attack angle of the specimen is 180° under ideal conditions

Table 3 Comparative table of natural frequencies

Vertical frequency (Hz)			Rotational frequency (Hz)			Horizontal frequency (Hz)		
Device in transiting test	Device in wind tunnel test	Percentage difference (%)	Device in transiting test	Device in wind tunnel test	Percentage difference (%)	Device in transiting test	Device in wind tunnel test	Percentage difference (%)
0.811	0.85	−4.59%	1.01	0.96	5.21%	1.10	1.54	28.57%

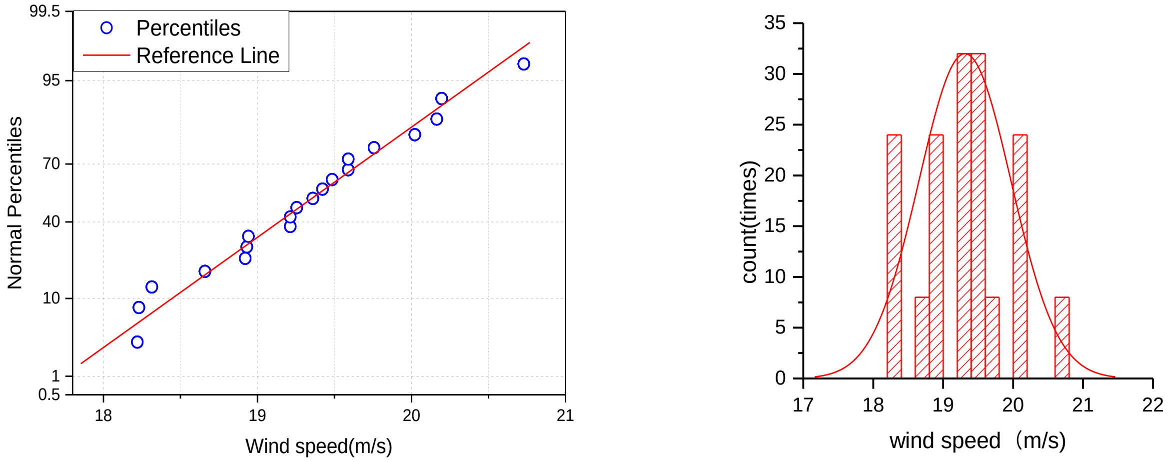

(a) Percentile bitmap of the wind speeds (b) Normal distribution of the wind speeds

Fig. 28 Wind speeds when the speed is at 72Km/h(20m/s)

So, when the indicated speed (v_1) is $72km/h$ (20m/s), the actual speed (v_2) shall conform to Eq. (11).

$$61.82km/h \le v_2 \le 72km/h \quad (11)$$

That is

$$61.82km/h \le v_2 \le 72km/h \quad (12)$$

In order to analyze the relationship between the driving speed and the wind speed generated by the moving vehicle, the experiment has been done in the ideal conditions (see Table 1) before beginning the experiments for aerodynamic coefficient and galloping. In this experiment, a total of 160 tests are carried out when the speed is 72 km/h (20 m/s) and the collection time interval is 30 s. According to Section 3.4.1, the driving wind field is stable in the transiting test, the external factors contributed relatively less interference under ideal conditions, and the measurement method of air velocity by the Pitot tube is practicable. As shown in Fig. 28, the speed can be obtained by Eq. (4), and the air density ρ is 1.186 kg/m³ based on the testing conditions. The average speed is 19.310 m/s, and the standard deviation is 0.660. Therefore, the confidence level within the range of 17.99 m/s to 20 m/s measured by Pitot tube is 95% under ideal conditions, and the result is fully satisfied by Eq. (10), as required by the standard.

5.2 Critical wind velocities

The preceding analysis reveals that the size of the iced conductor specimen for galloping measurements is identical with that of the benchmark model size adopted in reference (Chabart *et al.* 1998). The critical wind speed of galloping in the wind tunnel test is 8.5 m/s at 180°. However, the critical vehicular speed of galloping in the transiting test in this study is 47 km/h (13.056 m/s). According to Section 5.1, the wind speed measured by the Pitot tube is in the range of 11 m/s to 13 m/s, and the confidence level is 95% under ideal conditions. Apart from material and model size mentioned in Section 3.4.3, the difference of the critical wind velocities for the galloping of the specimen includes the following aspects.

(1) The vertical, rotational, and horizontal frequencies are different. Table 3 presents the differences between the two devices.

(2) The ideal circumstances. The selected driving sections satisfy the ideal test conditions required in this study. However, the external factors of the outdoor experiments, such as the surrounding traffic, the smoothness of the road, the outdoor temperature, and humidity, remain inevitable and may affect the experimental results.

In summary, the primary reason for the difference of the critical wind velocities for the galloping of the specimen between the transiting test and wind tunnel test is the differences between the test devices and the test specimens, and the secondary reason is the external factors of the outdoor experiments. In-depth research on the external factors will be thoroughly performed.

6. Conclusions

In the present work, the theoretical formula of transiting test is developed based on theoretical derivation and field test. The basic and special software and hardware systems of transiting test method for aerodynamic coefficient measurements and galloping of iced conductor are designed and assembled, respectively. The transiting test method is adopted, and several important conclusions are drawn from preceding considerations mentioned as follows.

(1) The theoretical formula of the transiting test method for aerodynamic coefficient measurements of iced conductor derived in the study is accurate, simple, and reasonable.

(2) The measurement method of air velocity by the Pitot tube is practicable. The driving wind field is stable in the transiting test, and has relatively less interference from external factors under ideal conditions, and can be considered in the experimental investigation of wind-resistant structures.

(3) The inertial force generated by the vehicular vibration is extremely small and negligible relative to aerodynamic force under ideal conditions.

(4) The aerodynamic coefficient curves of lift and drag in this study are compared with those of other studies. The changing trends of curves are basically the same, which confirms the feasibility of the proposed methods.

(5) Galloping phenomenon is observed in the transiting tests. As the speed increases, the time to maximum amplitude tends to occur early, the amplitude gradually increases, and the distance gradually becomes farther away from the end of the limit hole.

(6) Several errors exist in the wind speed measured by the Pitot tube and the vehicular speed when studying the galloping of iced conductor via the transiting test method. The actual wind speed should be measured in each testing condition. The method and apparatus perfectly accord with the results of previous studies.

Acknowledgments

The authors are grateful for the financial support from the National Natural Science Foundation of China (51778587, 51808510), Natural Science Foundation of Henan Province of China (162300410255), Supported by Foundation for University Young Key Teacher by Henan Province (2017GGJS005), Outstanding Young Talent Research Fund of Zhengzhou University (1421322059) and Science and technology planning project of Transportation in Henan Province (2016Y2-2, 2018J3).

References

Alonso, G., Meseguer, J. and Pérez-Grande, J. (2007), "Galloping stability of triangular cross-sectional bodies: a systematic approach". *J. Wind Eng. Ind. Aerod.*, **95**(9-11), 928~940.

Altinisik, A. (2017), Aerodynamic coastdown analysis of a passenger car for various configurations. *Int. J. Automot. Technol*., **18**(2), 245-254.

An, Y., Wang, C., Li, S. and Wang, D. (2016), "Galloping of steepled main cables in long-span suspension bridges during construction", *Wind Struct.*, **23**(6), 595-613

Blocken, B. and Toparlar, Y. (2015), "A following car in influences cyclist drag: CFD simulations and wind tunnel measurements", *J. Wind Eng. Ind. Aerod.*, **145,** 178-186.

Burdzik, R., Konieczny, Ł., Warczek, J. and Cioch, W. (2017), "Adapted linear decimation procedures for TFR analysis of non-stationary vibration signals of vehicle suspensions", *Mech. Res. Commun.*, **82**, 29-35.

Cai, M., Yan, B., Lu, X. and Zhou, L. (2015), "Numerical simulation of aerodynamic coefficients of iced-quad bundle conductors", *IEEE T. Power Delivery*, **30**(4), 1669-1676.

Chabart, O. and Lilien, J.L. (1998), "Galloping of electrical lines in wind tunnel facilities", *J. Wind Eng. Ind. Aerod.*, **98**, 967-976.

Chen, W., Zhang, Q., Li, H. and Hu, H. (2015), "An experimental investigation on vortex induced vibration of a flexible inclined cable under a shear flow", *J. Fluids Struct.*, **54**, 297-311.

Choi, C.C. and Kwon, D.K. (1998), "Wind tunnel blockage effects on aerodynamic behavior of bluff body", *Wind Struct.*, **1**(4), 351-364.

Den Harttog, J.P. (1932), "Transmission line vibration due to sleet", *AIEE Transaction*, **54**(4), 1074-1086

Feng, R.; Liu, F., Cai, Q., Yan, G. and Keng, J. (2018), "Field measurements of wind pressure on an open roof during Typhoons HaiKui and SuLi", *Wind Struct.*, **26**(1), 11-24.

Guo, P., Li, S. and Wang, D. (2019), "Effects of aerodynamic interference on the iced straddling hangers of suspension bridges by wind tunnel tests", *J. Wind Eng. Ind. Aerod.*, **184**, 162-173.

Guo, P., Li, S., Wang, C., Hu, Y. and Wang, D. (2017), "Influence of catwalk design parameters on the galloping of constructing main cables in long-span suspension bridges", *J. Vibroeng.*, **19**(6), 1392-8716.

Keutgen, R. and Lilien, JL. (2000), "Benchmark cases for galloping with results obtained from wind tunnel facilities validation of a finite element model", *IEEE T. Power Deliver.*, **15**,(1), 367-374.

Khayrullina, A.A., Blocken, B.B., Janssen, W. and Straathof, J. (2015), "CFD simulation of train aerodynamics: train-induced wind conditions at an underground railroad passenger platform", *J. Wind Eng. Ind. Aerod.*, **139**, 100-110.

Knight, J.J., Lucey, A.D. and Shaw, C.T. (2010), "Fluid-structure interaction of a two-dimensional membrane in a flow with a pressure gradient with application to convertible car roofs", *J. Wind Eng. Ind. Aerod.*, **98**(2), 65-72.

Li, S. and Zheng, S. (2017), "Aerodynamic performance analysis of wind-sand flow on riding-type hangers of suspension bridges", *J. Vibroeng.*, **19**(2), 1301-1313.

Li, S., An, Y., Wang, C. and Wang, D. (2017), "Experimental and numerical studies on galloping of the flat-topped main cables for the long span suspension bridge during construction", *J. Wind Eng. Ind. Aerod.*, **163**, 23-32.

Ma, W.Y., Liu, Q.K., Du, X.Q. and Wei, Y.Y. (2015), "Effect of the Reynolds number on the aerodynamic forces and galloping instability of a cylinder with semi-elliptical cross sections", *J. Wind Eng. Ind. Aerod.*, **146**, 71-80.

Nigol, O. and Buchan, P.G. (1981), "Conductor galloping-part I Den hartog mechanism", *IEEE T. Power Apparat. Syst.*, **100**(2), 699-707.

Nigol, O. and Clarke, G.J. (1974), "Conductor galloping and control based on torsional mechanism", *IEEE Power Engineering Society Winter Meeting Paper*. New York, No. C74016-2.

Shirai, S. and Ueda, T. (2003), "Aerodynamic simulation by CFD on flat box girder of super-long-span suspension bridge", *J. Wind Eng. Ind. Aerod.*, **91**, 279-290.

Skrúcaný, T., Semanová, S., Martin, K., Tomasz, F. and Ján, V. (2018), "Measuring mechanical resistances of a heavy good vehicle by coastdown test", *Adv. Sci. Technol. Res. J.*, **12**(2), 214-221.

Speed meters for motor vehicle. GB 15082-2008. Chinese Standards (GB).

Tao, L., Du, G., Liu, L., Liu, Y. and Shao, Z. (2015), "Experimental study and finite element analysis of wind-induced vibration of modal car based on fluid-structure interaction", *J. Hydrodynam.*, **25**, 118-124.

Wang, G.X., Hu, Y., Xu, T.T., Li, J.F. and Yang, B. (2013), "Numerical simulation and wind tunnel experiment of the aerodynamic characteristics of a formula student racing car", *Adv. Mater. Res*., 460-464.

Wang, H., Li, A., Niu, J., Zong, Z. and Li, J. (2013), "Long-term monitoring of wind characteristics at Sutong Bridge site", *J. Wind Eng. Ind. Aerod.*, **115**, 39-47.

Wang, X., Lou, W., Shen, G. and Xu, F. (2011), "A wind tunnel study on aerodynamic characteristics of iced conductor", *Acta Aerodynam. Sinica*, **29**(5), 573-579.

Wen, Q., Hua, X.G., Lei, X., Chen, Z.Q. and Niu, H.W. (2018), "Experimental study of wake-induced instability of coupled parallel hanger ropes for suspension bridges", *Eng. Struct.*, **167**, 175-187.

Xu, F., Wu, T., Ying, X. and Kareem, A. (2015), "Higher-order self-excited drag forces on bridge decks", *J. Eng. Mech.* **142**(3), 06015007.

Yan, Z., Savory, E., Li, Z. and Lin, W.E. (2014), "Galloping of iced quad-conductors bundles based on curved beam theory", *J. Wind Eng. Ind. Aerod.*, **127**, 59-68.

Yang, N., Zheng, X.K., Zhang, J., Law, S.S. and Yang, Q. (2015), "Experimental and numerical studies on aerodynamic loads on an overhead bridge due to passage of high-speed train", *J. Wind Eng. Ind. Aerod.*, **140**, 19-33.

Yousef, M.A.A, Selvam, P.R. and Prakash, J. (2018), "A comparison of the forces on dome and prism for straight and tornadic wind using CFD model", *Wind Struct.*, **26**(6), 369-382.

Zhou, L., Yan, B., Zhang, L. and Zhou, S. (2016), "Study on galloping behavior of iced eight bundle conductor transmission lines", *J. Sound Vib.*, **362**, 85-110.

CC